



# Vacuum polarization energy of the Shifman–Voloshin soliton

H. Weigel<sup>a,\*</sup>, N. Graham<sup>b</sup>

<sup>a</sup> Institute for Theoretical Physics, Physics Department, Stellenbosch University, Matieland 7602, South Africa

<sup>b</sup> Department of Physics, Middlebury College, Middlebury, VT 05753, USA



## ARTICLE INFO

### Article history:

Received 20 June 2018

Accepted 13 July 2018

Available online 17 July 2018

Editor: A. Ringwald

## ABSTRACT

We compute the vacuum polarization energy of soliton configurations in a model with two scalar fields in one space dimension using spectral methods. The second field represents an extension of the conventional  $\phi^4$  kink soliton model. We find that the vacuum polarization energy destabilizes the soliton except when the fields have identical masses. In that case the model is equivalent to two independent  $\phi^4$  models.

© 2018 The Author(s). Published by Elsevier B.V. This is an open access article under the CC BY license (<http://creativecommons.org/licenses/by/4.0/>). Funded by SCOAP<sup>3</sup>.

## 1. Introduction

Two-field models supporting solitons in one space dimension obtainable as Bogomol'nyi–Prasad–Sommerfeld (BPS) solutions have been considered in the context of a number of applications, including supersymmetry and domain walls, see [1–7] and references therein. The essential feature leading to these applications is that in one space dimension the soliton has a localized kink shape, which becomes a surface (domain wall) when embedded in higher dimensions. When two (or more) fields interact multiple kinks at finite separation(s) emerge. The BPS construction is then carried out by writing a superpotential for the fields. The simplest such model has been introduced by Bazeia et al. [4] who also constructed some of its soliton solutions, while the full spectrum of solitons, including numerical simulations, was uncovered by Shifman and Voloshin [6]. In Ref. [8] the analytically known solitons of this model were considered as an illustration of general techniques allowing for the extension of scattering theory methods for computing one-loop quantum corrections [9] to the case of models with a mass gap, which then have multiple thresholds in the scattering problem. Such corrections were computed in that model for the simple cases where the soliton does not couple the fluctuation modes of the two fields in Ref. [10] and for small and moderate separation of the kinks in Refs. [11,12] using heat kernel methods [13].

In this Letter, we apply the methods of Ref. [8] to study these quantum corrections in more detail by going beyond the analytically known solitons for this particular model, which we define following the approach and conventions of Ref. [4]. We show that

quantum corrections can significantly alter the classical stability of solitons in this model. In particular, the model can become unstable to the formation of a kink–antikink pair separated by a large region of *secondary* vacuum, whose classical energy density equals that of the *primary* vacuum outside the kink–antikink pair, but whose one-loop quantum energy density is negative.

The Bazeia model extends the  $\phi^4$  model by a second scalar field  $\chi$ . Its Lagrangian reads

$$\mathcal{L} = \frac{1}{2} [\partial_\nu \phi \partial^\nu \phi + \partial_\nu \chi \partial^\nu \chi] - \frac{\lambda}{4} \left[ \phi^2 - \frac{M^2}{2\lambda} + \frac{\mu}{2} \chi^2 \right]^2 - \frac{\lambda}{4} \mu^2 \chi^2 \phi^2. \quad (1)$$

The Lagrangian contains the typical coupling constant  $\lambda$  and the mass scale  $M$  as in the conventional  $\phi^4$  model. We will discuss the meaning of the dimensionless coupling constant  $\mu$  shortly. First we note that in the case  $\mu = 2$ , when the two fields are indistinguishable, the orthogonal transformation  $\varphi_{1,2} = \frac{1}{\sqrt{2}} [\chi \pm \phi]$  decouples the model into

$$\left[ \phi^2 - \frac{M^2}{2\lambda} + \chi^2 \right]^2 + \lambda \chi^2 \phi^2 = 2 \left[ \varphi_1^2 - \frac{M^2}{4\lambda} \right]^2 + 2 \left[ \varphi_2^2 - \frac{M^2}{4\lambda} \right]^2,$$

which is a sum of two conventional and identical  $\phi^4$  models. As a result, the known results [15] from the  $\phi^4$  model with its kink soliton solution will provide checks of our calculations.

There are two distinct vacuum configurations. First, the solution with  $\phi = \pm M/\sqrt{2\lambda}$  and  $\chi = 0$ , adopted from the  $\phi^4$  model, and second, the solution with  $\phi = 0$  and  $\chi = \pm M/\sqrt{\mu\lambda}$ . Later we will see that only the first allows for BPS soliton solutions unless  $\mu = 2$ , and thus we refer to it as the *primary* vacuum and the second as the *secondary* vacuum. The masses for fluctuations around

\* Corresponding author.

E-mail addresses: [weigel@sun.ac.za](mailto:weigel@sun.ac.za) (H. Weigel), [ngraham@middlebury.edu](mailto:ngraham@middlebury.edu) (N. Graham).

the primary vacuum are  $m_\phi = M$  and  $m_\chi = \mu M/2$ . That is, the dimensionless coupling constant is twice the ratio of the two masses.

After appropriate redefinition of the fields,  $(\phi, \chi) \rightarrow (M/\sqrt{2\lambda})(\phi, \chi)$  and the coordinates,  $x_v \rightarrow 2x_v/M$  the rescaled Lagrangian,  $\mathcal{L} \rightarrow (M^4/8\lambda)\mathcal{L}$  is conveniently expressed as

$$\mathcal{L} = \frac{1}{2} [\partial_\nu \phi \partial^\nu \phi + \partial_\nu \chi \partial^\nu \chi] - U(\phi, \chi) \quad \text{with}$$

$$U(\phi, \chi) = \frac{1}{2} \left[ \phi^2 - 1 + \frac{\mu}{2} \chi^2 \right]^2 + \frac{\mu^2}{2} \phi^2 \chi^2. \quad (2)$$

In these units the primary vacuum configuration is  $\phi_{\text{vac}} = \pm 1$  and  $\chi_{\text{vac}} = 0$  so that  $m_\chi = \mu$  and  $m_\phi = 2$ . Note that with these dimensionless variables the classical mass is measured in units of  $M^3/\lambda$ , while the one-loop quantum energy, which is central to the current study, scales with  $M/m_\phi$ . The different scales arise from the overall loop-counting factor in  $\mathcal{L}$  that emerges from canonical quantization.

In Section 2 we describe the construction of the solitons in this model. Following, in Section 3, we review the computation of the one-loop quantum, or vacuum polarization energy (VPE) in the no-tadpole renormalization scheme. In Section 4 we present the numerical results for the VPE and show that it produces an instability unless  $\mu = 2$ . We conclude in Section 5. In an Appendix we show that the finite renormalization imposing on-shell conditions does not alter the conclusion of instability.

## 2. Soliton

The Bazeia model [4] is defined to allow a BPS construction for the classical energy

$$E_{\text{cl}} = \frac{1}{2} \int_{-\infty}^{\infty} dx \left[ \phi'^2 + \chi'^2 + \left( \phi^2 - 1 + \frac{\mu}{2} \chi^2 \right)^2 + \mu^2 \phi^2 \chi^2 \right]$$

$$= \frac{1}{2} \int_{-\infty}^{\infty} dx \left[ \left( \phi^2 - 1 + \frac{\mu}{2} \chi^2 \pm \phi' \right)^2 + (\mu \phi \chi \pm \chi')^2 \right]$$

$$\pm \left[ \phi - \frac{1}{3} \phi^3 - \mu \phi \chi^2 \right]_{-\infty}^{\infty}, \quad (3)$$

where the prime denotes the derivative with respect to the (dimensionless) coordinate  $x$ . We immediately see that only profile functions that assume the primary vacuum configuration can have finite non-zero energy.<sup>1</sup> Choosing  $\phi(\pm\infty) = \pm 1$  requires the upper sign in Eq. (3) because  $\phi(x)$  must (monotonically) increase. Then the BPS equations read

$$\frac{d\chi(x)}{dx} = -\mu\phi(x)\chi(x) \quad \text{and}$$

$$\frac{d\phi(x)}{dx} = 1 - \phi^2(x) - \frac{\mu}{2}\chi^2(x). \quad (4)$$

These coupled differential equations have been studied in detail by Shifman and Voloshin [6]. For completeness we discuss those results. The model exhibits translational invariance and we center the (eventual) soliton at  $x_0 = 0$ . Then  $\chi$  and  $\phi$  are symmetric and anti-symmetric functions, respectively,<sup>2</sup> and so  $\phi(0) = 0$  and  $\chi'(0) = 0$ . We are free to choose  $\chi(0) \geq 0$ . If  $\chi(0) > \sqrt{2/\mu}$ ,  $\phi'(0) < 0$  so that  $\phi(0^+) < 0$ . In turn  $\chi$  would increase and  $\chi(0)$

**Table 1**  
Analytically known soliton solutions [4,6].

	$\phi(x)$	$\chi(x)$	Parameters
I)	$\tanh(x)$	0	$a = 0$
II)	$\tanh(\mu x)$	$\frac{\sqrt{2(1/\mu-1)}}{\cosh(\mu x)}$	$\mu < 1, a = \sqrt{1-\mu}$
III)	$\frac{\sinh(2x)}{b+\cosh(2x)}$	$\frac{\sqrt{b^2-1}}{b+\cosh(2x)}$	$\mu = 2, b = \frac{1+a^2}{1-a^2}$
IV)	$\frac{(1-a^2)\sinh(x)}{a^2+(1-a^2)\cosh(x)}$	$\frac{2a}{\sqrt{a^2+(1-a^2)\cosh(x)}}$	$\mu = \frac{1}{2}$

would be a minimum. Furthermore  $\phi'$  would turn even more negative and not approach  $+1$  at spatial infinity. By contradiction we thus conclude that  $\sqrt{2/\mu}$  is an upper bound for  $\chi(0)$  and we parameterize  $\chi(0) = a\sqrt{2/\mu}$  with  $0 \leq a < 1$ . An equivalent bound was derived in Ref. [6] from the condition that the solution to

$$\frac{d\phi^2}{d\chi} = 2\phi \frac{d\phi}{d\chi} \left( \frac{d\chi}{dx} \right)^{-1} = -\frac{2 - 2\phi^2 - \mu\chi^2}{\mu\chi}$$

is consistent with  $\phi^2 \geq 0$ .

Because of the reflection symmetry  $x \leftrightarrow -x$  it is sufficient to solve Eqs. (4) on the half-line  $x \geq 0$ . In the numerical simulation we initialize  $\phi(0) = 0$  and  $\chi(0) = a\sqrt{2/\mu}$  and vary  $a$ . For any numerical solution we then verify that the first integral in Eq. (3) produces  $E_{\text{cl}} = \frac{4}{3}$ . We also verify that the numerical solutions agree with the analytically known results listed in Table 1.

We thus find that the various known analytical solutions are not independent but are related by a single parameter. If these solitons were independent, a third zero mode for the small amplitude fluctuations about the soliton along the direction in field space connecting the solutions would have emerged, but only two have been observed [8]. Stated otherwise, the solitons are parameterized by two continuous parameters [6]: the center of the soliton, which we set to zero, and the amplitude of the  $\chi$  field, which we parameterize by  $a$ . Varying these parameters produces the two observed zero modes. Alternatively, the family of solitons can be constructed by successively adding infinitesimal contributions proportional to the zero mode wave-function.

The limit  $a \rightarrow 1$  deserves further discussion. In that case, the right-hand-sides of Eq. (4) are tiny in a wide region around  $x = 0$ , so that the profiles stay constant at their  $x = 0$  values. Eventually two well separated structures emerge at which  $\phi$  changes from  $-1$  to zero and zero to  $+1$ , respectively [6]. Simultaneously,  $\chi$  changes from zero to  $a\sqrt{2/\mu}$  and back to zero. We show this behavior in Fig. 1 (where we only display the  $x \geq 0$  regime since the profiles are obtained by reflection for  $x \leq 0$ ). When  $a \rightarrow 1$ ,  $\chi(0)$  approaches  $\sqrt{2/\mu}$  and the slope  $\phi'(0)$  decreases so that the profiles assume the secondary vacuum configuration in a large range of coordinate space.

While  $\mu$  is a model parameter,  $a$  is a variational parameter that we tune to minimize the total energy. Since  $E_{\text{cl}}$  does not depend on  $a$ , we only need to consider the  $a$  dependence of the VPE, whose formulation we discuss next.

## 3. Vacuum polarization energy

The computation of the vacuum polarization energy in models with a mass gap ( $\mu \neq 2$ ) has been established in Ref. [8]. We briefly summarize it here. The central input is the Jost function for imaginary momenta  $t = ik$ . The starting point for its computation is the second order differential equation

$$Z''(t, x) = 2Z'(t, x)D(t) + M^2Z(t, x) - Z(t, x)M^2 + V(x)Z(t, x)$$

$$\text{with } M^2 = \begin{pmatrix} \mu^2 & 0 \\ 0 & 4 \end{pmatrix} \quad (5)$$

<sup>1</sup> For  $\mu = 2$  an alternative BPS construction is possible producing a soliton with  $\lim_{|x| \rightarrow \infty} \chi(x) \neq 0$ .

<sup>2</sup> Eqs. (4) also allow the opposite choice; but then the energy, Eq. (3) is zero.

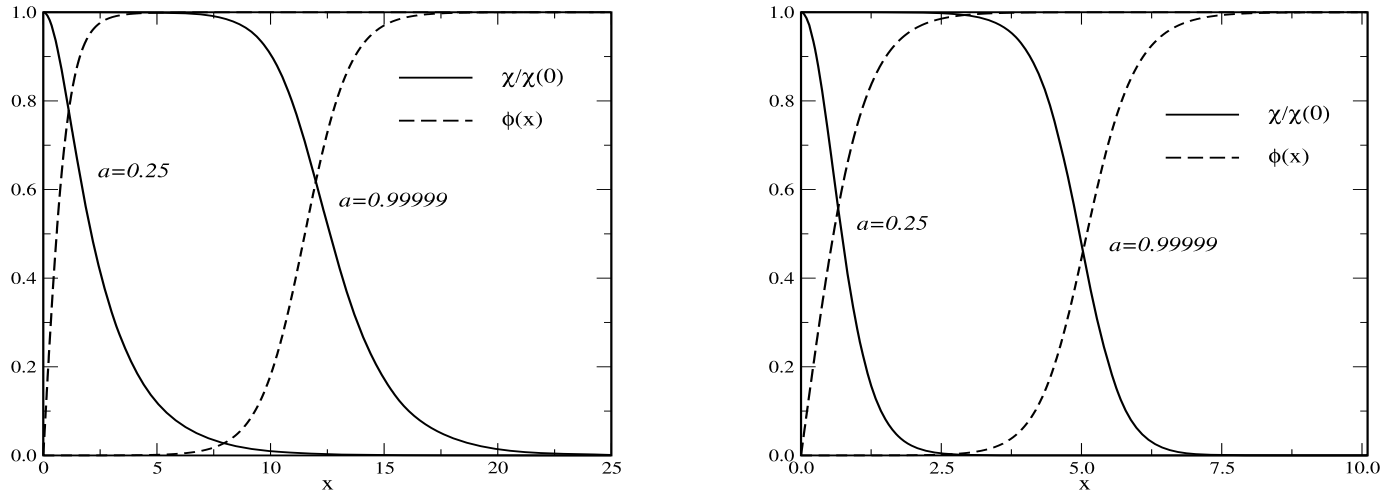


Fig. 1. Soliton profiles for  $\mu = 0.5$  (left panel) and  $\mu = 3.0$  (right panel). Note the different scales on the horizontal axes.

and

$$D(t) = \begin{pmatrix} t_1 & 0 \\ 0 & t_2 \end{pmatrix}, \quad \text{where} \quad (6)$$

$$(t_1, t_2) = \begin{cases} (t, \sqrt{t^2 - \mu^2 + 4}) & \text{for } \mu \leq 2 \\ (\sqrt{t^2 - 4 + \mu^2}, t) & \text{for } \mu \geq 2. \end{cases}$$

The scattering problem is defined via the potential matrix

$$V(x) \equiv \partial^2 U - M^2 = \begin{pmatrix} \mu(1 + \mu)(\phi^2 - 1) + \frac{3}{2}\mu^2\chi^2 & 2\mu(1 + \mu)\chi\phi \\ 2\mu(1 + \mu)\chi\phi & 6\phi^2 - 6 + \mu(\mu + 1)\chi^2 \end{pmatrix}, \quad (7)$$

with the soliton profiles  $\phi = \phi(x)$  and  $\chi = \chi(x)$  obtained as (numerical) solutions to Eq. (4) substituted. We solve the matrix equations (5) with the boundary conditions  $\lim_{x \rightarrow \infty} Z(t, x) = \mathbb{1}$  and  $\lim_{x \rightarrow \infty} Z'(t, x) = 0$  and extract the Jost matrices

$$F_S(t) = \lim_{x \rightarrow 0} [Z(t, x) - Z'(t, x)D^{-1}(t)] \quad \text{and} \quad (8)$$

$$F_A(t) = \lim_{x \rightarrow 0} Z(t, x).$$

The reflection properties of the profiles lead to skewed parity,  $V(-x) = \begin{pmatrix} 1 & 0 \\ 0 & -1 \end{pmatrix} V(x) \begin{pmatrix} 1 & 0 \\ 0 & -1 \end{pmatrix}$  so that the decoupled Jost matrices are

$$F_{\pm}(t) = [P_{\pm} F_S(t) D_{\mp}(t) + P_{\mp} F_A(t) D_{\pm}^{-1}(t)], \quad (9)$$

with projectors  $P_+ = \begin{pmatrix} 1 & 0 \\ 0 & 0 \end{pmatrix}$ ,  $P_- = \begin{pmatrix} 0 & 0 \\ 0 & 1 \end{pmatrix}$  and the factor matrices

$$D_+(t) = \begin{pmatrix} -t_1 & 0 \\ 0 & 1 \end{pmatrix} \quad \text{and} \quad D_-(t) = \begin{pmatrix} 1 & 0 \\ 0 & -t_2 \end{pmatrix}.$$

From this we finally compute the appropriate Jost function for imaginary momenta

$$v(t) \equiv \ln \det [F_+(t) F_-(t)] \quad (10)$$

that enters the vacuum polarization energy

$$E_{\text{vac}} \equiv \int \frac{dt}{2\pi} \frac{t}{\sqrt{t^2 - m_0^2}} [v(t) - v^{(1)}(t)], \quad (11)$$

where  $m_0 = \min(\mu, 2)$ . The subtraction of the Born approximation

$$v^{(1)}(t) = \int_0^{\infty} dx \left[ \frac{V_{11}(x)}{t_1} + \frac{V_{22}(x)}{t_2} \right], \quad (12)$$

where  $V_{ij}$  refers to the elements of the potential matrix in Eq. (7), enforces the no-tadpole renormalization condition.

#### 4. Numerical results

With the formalism to compute the VPE of the two-field soliton now fully established, we list numerical results in Table II as a function of the model parameter  $\mu$  and the variational parameter  $a$ . For  $\mu = 2$ , there is no variation with  $a$ , because the  $\mu = 2$  model is merely a duplication of the kink model. Hence this case serves as a check of our numerical procedure, reproducing the known result  $E_{\text{vac}} = 1/\sqrt{3} - 6/\pi \approx -1.3325$  [14,15]. Our numerical results are also consistent with those from a heat kernel expansion. Though we observe differences of up to one percent compared to the earlier results [11], a subgroup of those authors has later modified the expansion for  $1.4 \leq \mu \leq 3.1$  in Refs. [10,12] and we agree with the data reported in Table 1 (with  $\gamma = a$  and  $\sigma = \mu$ ) of Ref. [12] to numerical precision. We also observe a shallow local minimum of the VPE for  $2 < \mu \leq 3.2$  and moderate  $a$ . However, this feature is not general for  $\mu \geq 2$ . Rather the minimum becomes shallower and its position moves to smaller  $a$  as  $\mu$  increases and fully disappears for  $\mu = 4.4$ . The results produced in Tables 4 and 5 of Ref. [10] suggest that the truncated heat kernel expansion is inaccurate for  $\mu \leq 1$ . Our spectral methods do not require any truncation and, in contrast to statements in Refs. [11, 12], they clearly show that indeed the DHN method [14] (generalizing scattering techniques) can be efficiently utilized to compute the VPE of the two-field soliton.

For large enough  $a$ , curve-fitting suggests a logarithmic divergence as  $a \rightarrow 1$ ,

$$E_{\text{vac}} \sim E_0 + E_1 \ln(1 - a), \quad (13)$$

where the constants  $E_0$  and  $E_1$  vary with  $\mu$ . We present our results for  $E_1$  in Table III. This logarithmic divergence signals the instability of the soliton. Regardless of the coupling constant  $\lambda$ ,

**Table II**

Numerical results for the vacuum polarization energy, Eq. (11), of the Shifman–Voloshin soliton. The  $a = 0$  results are from I) in Table I. The  $\mu = 0.5$  results have been obtained from both the analytical and numerical soliton solutions.

$a$	$\mu$											
	0.5	0.8	1.0	1.2	1.6	2.0	2.4	2.8	3.2	3.6	4.0	4.4
0.0	-0.830	-0.922	-0.985	-1.049	-1.186	-1.333	-1.491	-1.661	-1.844	-2.039	-2.246	-2.467
0.1	-0.833	-0.924	-0.986	-1.050	-1.186	-1.333	-1.491	-1.661	-1.843	-2.038	-2.246	-2.467
0.2	-0.841	-0.929	-0.990	-1.053	-1.187	-1.333	-1.490	-1.660	-1.842	-2.037	-2.245	-2.467
0.3	-0.856	-0.938	-0.997	-1.058	-1.189	-1.333	-1.489	-1.658	-1.840	-2.036	-2.245	-2.467
0.4	-0.878	-0.952	-1.007	-1.065	-1.192	-1.333	-1.487	-1.656	-1.839	-2.035	-2.247	-2.470
0.5	-0.906	-0.971	-1.020	-1.074	-1.195	-1.333	-1.486	-1.654	-1.837	-2.036	-2.249	-2.477
0.6	-0.949	-0.995	-1.037	-1.085	-1.199	-1.333	-1.484	-1.653	-1.838	-2.039	-2.257	-2.490
0.7	-1.007	-1.027	-1.059	-1.100	-1.204	-1.333	-1.483	-1.653	-1.841	-2.048	-2.273	-2.515
0.8	-1.089	-1.072	-1.089	-1.119	-1.210	-1.333	-1.482	-1.656	-1.851	-2.068	-2.304	-2.560
0.9	-1.229	-1.145	-1.135	-1.147	-1.217	-1.333	-1.484	-1.666	-1.876	-2.112	-2.372	-2.656
0.99	-1.661	-1.363	-1.271	-1.227	-1.235	-1.333	-1.496	-1.714	-1.978	-2.284	-2.628	-3.008
0.999	-2.076	-1.572	-1.401	-1.303	-1.251	-1.333	-1.510	-1.764	-2.083	-2.459	-2.888	-3.364
0.9999	-2.488	-1.781	-1.530	-1.379	-1.268	-1.333	-1.523	-1.813	-2.187	-2.634	-3.147	-3.720
0.99999	-2.900	-1.990	-1.660	-1.454	-1.284	-1.333	-1.536	-1.863	-2.291	-2.809	-3.406	-4.076

**Table III**

Coefficient of the logarithmic divergence in Eq. (13) fitted from  $a \geq 0.8$  data in Table II, and energy per unit length for step function potential, Eq. (14).

$\mu$	0.5	0.8	1.0	1.2	1.6	2.0	2.4	2.8	3.2	3.6	4.0	4.4
$E_1$	0.182	0.092	0.057	0.034	0.007	0	0.006	0.021	0.045	0.075	0.112	0.154
$E_B/x_0$	-0.178	-0.114	-0.079	-0.051	-0.013	0.0	-0.013	-0.051	-0.115	-0.204	-0.319	-0.459

there is always a value of  $a$  close enough to one such that the total energy is negative. Again, it is important to stress that  $a$  is a variational parameter of the soliton rather than a (fixed) model parameter like  $\lambda$  or  $\mu$ .

To understand the origin of the instability, we note that in the limit  $a \rightarrow 1$ , for a wide region of space ( $|x| \leq x_0$ ), the profiles equal their  $x = 0$  values. This actually is the secondary vacuum at  $\phi = 0$  and  $\chi = \sqrt{2/\mu}$  whose curvature differs from the primary vacuum at  $\phi = 1$  and  $\chi = 0$ . In that range, the potential matrix Eq. (7) can therefore be approximated by a (double) step function

$$V(x) \sim (\mu - 2) \begin{pmatrix} -\mu & 0 \\ 0 & 2 \end{pmatrix} \Theta(x_0 - |x|). \tag{14}$$

In this limit the two channels decouple and the vacuum polarization energy can be computed separately. Moreover, this limiting potential is symmetric under  $x \rightarrow -x$  and standard techniques yield [16]

$$E_B = \sum_{i=1,2} \int_{m_i}^{\infty} \frac{dt}{2\pi} \frac{t}{\sqrt{t^2 - m_i^2}} \times \left[ \ln \left\{ g_i(t, 0) \left( g_i(t, 0) - \frac{1}{t} g'_i(t, 0) \right) \right\} \right]_1, \tag{15}$$

where  $i = 1, 2$  refers to the two (decoupled) particles with  $m_1 = \mu$  and  $m_2 = 2$ . The subscript on the square brackets denotes the subtraction of the Born approximation in the no-tadpole renormalization condition. Since the potential matrix is diagonal,  $V = \text{diag}(V_{11}, V_{22})$ , the Jost solutions  $g_i(t, x)$  decouple and obey the differential equations

$$g''_i(t, x) = 2t g'_i(t, x) + V_{ii}(x) g_i(t, x) \tag{16}$$

subject to the boundary conditions  $g_i(t, \infty) = 1$  and  $g'_i(t, \infty) = 0$ . For the step-function potential of Eq. (14) the Jost functions are straightforwardly obtained to be [17]

$$g_i(t, 0) = \frac{\kappa_1^{(i)} e^{-\kappa_2^{(i)} x_0} - \kappa_2 e^{-\kappa_1^{(i)} x_0}}{\kappa_1^{(i)} - \kappa_2^{(i)}} \quad \text{and}$$

$$g'_i(t, 0) = \frac{\kappa_1^{(i)} \kappa_2^{(i)}}{\kappa_1^{(i)} - \kappa_2^{(i)}} \left( e^{-\kappa_2^{(i)} x_0} - e^{-\kappa_1^{(i)} x_0} \right), \tag{17}$$

with  $\kappa_{1,2}^{(i)} = t \pm \sqrt{t^2 + v_i}$ ,  $v_1 = \mu(2 - \mu)$  and  $v_2 = 2(\mu - 2)$ . For the kinematics required by the integral Eq. (15),  $t \geq \mu$  for  $i = 1$  and  $t \geq 2$  for  $i = 2$ , the  $\kappa_{1,2}^{(i)}$  are always real. This suggests that the limiting potential solely acts as a barrier for the purpose of the VPE, even though one of the diagonal components of  $V$  is attractive. We thus expect that the VPE becomes even more negative as we increase  $x_0$  [17]. Indeed numerically we find that for large  $x_0$  the ratio  $E_B/x_0$  approaches negative constants (varying with  $\mu$ ), which we also list in Table III. Of course, for large  $x_0$  the ratio  $E_B/x_0$  is nothing but the quantum energy density of the secondary vacuum. We have computed the correlation coefficient between  $E_1$  and  $E_B/x_0$  to be 0.8, *i.e.* quite significant. This is a first indication that the instability is caused by the solution spreading into the secondary vacuum. To further compare with the step function potential, Eq. (14), we first estimate the extension of the soliton as

$$x_S(a) = \frac{\int_0^{\infty} dx x \epsilon(x)}{\int_0^{\infty} dx \epsilon(x)} = \frac{3}{2} \int_0^{\infty} dx x \epsilon(x), \tag{18}$$

where  $\epsilon(x)$  is the energy density of the soliton, *i.e.* the integrand of the first integral in Eq. (3) with the soliton profiles for given value of  $a$  substituted. From this we obtain

$$\Delta E_B = E_B(x_S(0.99)) - E_B(x_S(0.99999)). \tag{19}$$

In Table IV we compare  $\Delta E_B$  with  $\Delta E_S$ , the latter being the difference between the  $a = 0.99$  and  $a = 0.99999$  entries in Table II. The coincidence (to numerical accuracy) between  $\Delta E_B$  and  $\Delta E_S$  clearly shows that the instability is caused by the expansion of the soliton into the secondary vacuum.

One might imagine that finite renormalizations required to implement an on-shell scheme could alter this conclusion. In the appendix we determine the counterterms for this scheme and show that the instability persists.

**Table IV**

Differences of vacuum polarization energies for soliton extensions (into the secondary vacuum) corresponding to  $a = 0.99$  and  $a = 0.99999$ . Top row: limiting potential, Eq. (14), bottom row: full potential with data taken from Table II.

$\mu$	0.5	0.8	1.0	1.2	1.6	2.4	2.8	3.2	3.6	4.0	4.4
$\Delta E_B$	1.242	0.627	0.390	0.228	0.049	0.040	0.149	0.313	0.527	0.779	1.072
$\Delta E_S$	1.239	0.627	0.390	0.227	0.049	0.040	0.149	0.313	0.525	0.777	1.068

## 5. Conclusion

For a well-established soliton model consisting of two real scalar fields in one space dimension, we have computed the one-loop quantum correction to the soliton energy for a complete set of soliton solutions. The model is defined in terms of three parameters, the coupling strength  $\lambda$  and the masses of the two fields. For simplicity we have scaled coordinates and fields such that  $\lambda$  only appears as an overall factor in the action but not in the field equations, which are only sensitive to the mass ratio. However, upon quantization the classical energies carry a relative factor of  $1/\lambda$  compared to the quantum energies. In this model, the soliton solutions are characterized by two variational parameters, the location of the soliton and the amplitude  $a < 1$  of the spatially symmetric profile function. While the classical energy does not vary with these parameters, the vacuum polarization energy diverges logarithmically to negative infinity as  $a \rightarrow 1$  unless the two masses are equal. We have employed (generalized) spectral methods [8,9] for this computation but note that our results are consistent with those obtained in a heat kernel expansion [10–12]. However, those studies did not identify the importance and origin of this divergence,<sup>3</sup> which implies that for any finite value of  $\lambda$ , we can find  $a \lesssim 1$  such that the total energy is negative, and hence the quantum corrections destabilize the solitons. We have seen that the instability is related to the existence of a *secondary* vacuum. While this configuration is classically degenerate with the *primary* vacuum, its curvatures in field space, *i.e.* the masses of the fluctuating fields, are different, as given by the matrix in Eq. (14). As  $a \rightarrow 1$ , the soliton profiles contain larger and larger regions of the secondary vacuum, thereby reducing the vacuum polarization energy. We have confirmed this feature by comparison with the vacuum polarization energy of a step function background simulating the transition between the two vacua.

The situation is similar to the  $\varphi^6$  model with  $U_6 = \frac{1}{2}(\varphi^2 + \alpha^2)(\varphi^2 - 1)^2$ ; in that case the range of the secondary vacuum is measured by the model parameter  $\alpha$  and the vacuum polarization energy diverges as  $\alpha \rightarrow 0$  [17,18]. In that model the primary vacua are at  $\varphi = \pm 1$  and soliton solutions connect these vacua between negative and positive spatial infinity. As  $\alpha \rightarrow 0$  a secondary vacuum emerges at  $\varphi = 0$  and the soliton assumes that value<sup>4</sup> in a range of space that increases with  $1/\alpha$ . Together with the current study this suggests that quantum instabilities of solitons emerge as a generic feature whenever there is a secondary vacuum.

As a next step it will be interesting to see whether this instability persists when embedding this one space dimension model into higher dimensions, *i.e.* whether domain walls constructed from this model will also be unstable. This investigation can be pursued along the line of the interface formalism [20]. With additional quantum fluctuations in the transverse directions, the vacuum polarization energy per unit length/area will be altered, while the

classical energy (also per unit length/area) will remain unchanged because it is a local quantity.

## Acknowledgements

The authors very much appreciate helpful discussions with M. Quandt at an early stage of this project. H.W. is supported in part by the National Research Foundation of South Africa (NRF) by grant 109497. N.G. is supported in part by the National Science Foundation (NSF) through grant PHY-1520293.

## Appendix A. Effective action and renormalization

We determine the counterterms for on-shell renormalization from the one-loop effective action

$$\mathcal{A}_{\text{eff}} = \frac{i}{2} \text{Tr} \ln [1 + G^{-1} V] \quad \text{where} \quad G = \partial_\mu \partial^\mu + M^2 \quad (\text{A.1})$$

is the mass matrix defined in Eq. (5) and  $V$  is the potential matrix from Eq. (7). The trace in Eq. (A.1) goes over the two particle species and space–time. Only the contribution linear in  $V$  is ultraviolet divergent. In  $D = 2 - 2\epsilon$  space–time dimensions,<sup>5</sup> this linear term becomes

$$\begin{aligned} \mathcal{A}_{\text{eff}}^{(1)} = & -\frac{1}{8\pi} \left[ \frac{1}{\epsilon} - \gamma - \ln \frac{\mu^2}{4\pi^2 \Lambda^2} \right] \int d^2x V_{11} \\ & - \frac{1}{8\pi} \left[ \frac{1}{\epsilon} - \gamma - \ln \frac{4}{4\pi^2 \Lambda^2} \right] \int d^2x V_{22}, \end{aligned} \quad (\text{A.2})$$

where  $\Lambda$  is a renormalization scale (which is dimensionless in the present conventions). In this divergent term the fields appear at most quadratically and we need the two counterterms

$$\mathcal{L}_{\text{ct}}^{(1)} = c_1 (\phi^2 - 1) + c_2 \chi^2, \quad (\text{A.3})$$

with

$$\begin{aligned} c_1 = & \frac{1}{8\pi} \left\{ \mu(\mu + 1) \left[ \frac{1}{\epsilon} - \gamma - \ln \frac{\mu^2}{4\pi^2 \Lambda^2} \right] \right. \\ & \left. + 6 \left[ \frac{1}{\epsilon} - \gamma - \ln \frac{4}{4\pi^2 \Lambda^2} \right] \right\} \\ c_2 = & \frac{1}{8\pi} \left\{ \frac{3}{2} \mu^2 \left[ \frac{1}{\epsilon} - \gamma - \ln \frac{\mu^2}{4\pi^2 \Lambda^2} \right] \right. \\ & \left. + \mu(\mu + 1) \left[ \frac{1}{\epsilon} - \gamma - \ln \frac{4}{4\pi^2 \Lambda^2} \right] \right\}. \end{aligned} \quad (\text{A.4})$$

Note that these counterterms do not form part of the original Lagrangian, Eq. (1), preventing a direct multiplicative renormalization. However, the only purpose of this counterterm is to exactly compensate the local tadpole diagram contribution to the action, Eq. (A.2), which is represented by the Born approximation, Eq. (12), in the VPE. Hence this counterterm will cancel in the total energy.

<sup>3</sup> In Ref. [11] it was concluded that the VPE would be almost constant for a wide range of  $a$ . This is indeed true for  $\mu \approx 2$  and  $a$  not too close to one, but is not the case otherwise.

<sup>4</sup> For  $\alpha = 0$  two solitons exist [19]; one connects  $\phi = -1$  to  $\phi = 0$  and the other  $\phi = 0$  to  $\phi = 1$ . The  $\alpha \neq 0$  version combines these transitions. As  $\alpha$  increases, their overlap within the secondary vacuum decreases.

<sup>5</sup> The equivalence with the Born result, Eq. (12) has been established in Ref. [21] for arbitrary dimensions.

To implement the physical on-shell scheme we define fluctuations  $\eta_i$  about the primary vacuum via  $\phi = 1 + \eta_1$  and  $\chi = 0 + \eta_2$ . The counterterms

$$\begin{aligned} \mathcal{L}_{\text{ct}}^{(2)} &= -d_1 \left( \phi^2 - 1 + \frac{\mu}{2} \chi^2 \right)^2 \\ &\quad - d_2 (\chi \phi)^2 + d_3 \partial_\mu \phi \partial^\mu \phi + d_4 \partial_\mu \chi \partial^\mu \chi \\ &= -4d_1 \eta_1^2 - d_2 \eta_2^2 + d_3 \partial_\mu \eta_1 \partial^\mu \eta_1 + d_4 \partial_\mu \eta_2 \partial^\mu \eta_2 \\ &\quad + \mathcal{O}(\eta_i^3) \end{aligned} \tag{A.5}$$

compensate for any quantum correction to the positions and residues of the  $\eta_i$  propagators. We stress that  $\mathcal{L}_{\text{ct}}^{(2)}$  contains exactly the terms of the original Lagrangian, Eq. (1). That is, the on-shell scheme can indeed be implemented by multiplicative renormalization, at least at one loop order. This counterterm will contribute

$$\begin{aligned} E_{\text{ct}} &= d_1 \int dx \left( \phi^2 - 1 + \frac{\mu}{2} \chi^2 \right)^2 + \frac{d_2}{\mu^2} \int dx (\mu \chi \phi)^2 \\ &\quad + d_3 \int dx \phi'^2 + d_4 \int dx \chi'^2 \end{aligned} \tag{A.6}$$

to the total energy. When substituting the soliton configuration, Derrick's theorem tells us that

$$\begin{aligned} \frac{1}{2} \int dx \left[ \left( \phi^2 - 1 + \frac{\mu}{2} \chi^2 \right)^2 + (\mu \chi \phi)^2 \right] &= \frac{1}{2} \int dx [\phi'^2 + \chi'^2] \\ &= \frac{2}{3}. \end{aligned}$$

Hence each of the integrals in Eq. (A.6) is bounded between zero and  $\frac{4}{3}$ . By renormalizability, the coefficients  $d_i$  do not depend on the profiles. Hence  $E_{\text{ct}}$  will only contribute a finite amount to the total energy in the limit  $a \rightarrow 1$  and thus its addition does not prevent the instability.

For completeness we determine the finite coefficients  $d_i$  from the second order effective action  $\mathcal{A}_{\text{eff}}^{(2)} = -\frac{1}{4} \text{Tr} [G^{-1} V G^{-1} V]$ . To compare with the expanded form in Eq. (A.5) it suffices to consider the linear terms in  $V$ :

$$V = \begin{pmatrix} 2\mu(\mu+1)\eta_1 & 2\mu(\mu+1)\eta_2 \\ 2\mu(\mu+1)\eta_2 & 12\eta_1 \end{pmatrix} + \mathcal{O}(\eta_i^2).$$

Performing the loop integrals yields

$$\begin{aligned} \mathcal{A}_{\text{eff}}^{(2)} &= \frac{1}{4\pi} \int \frac{d^2 k}{2\pi} \left\{ \left[ \mu^2(\mu+1)^2 I(k^2, 2, 2) + 36 I(k^2, \mu, \mu) \right] \right. \\ &\quad \times \tilde{\eta}_1(k) \tilde{\eta}_1(-k) \\ &\quad \left. + 2\mu^2(\mu+1)^2 I(k^2, 2, \mu) \tilde{\eta}_2(k) \tilde{\eta}_2(-k) \right\} \end{aligned} \tag{A.7}$$

where  $\tilde{\eta}_i(k) = \int d^2 x e^{ik \cdot x} \eta_i(x)$  are Fourier transforms and

$$I(k^2, m_1, m_2) = \int_0^1 \frac{dx}{m_1^2 - x(m_1^2 - m_2^2) - x(1-x)k^2}$$

is a Feynman parameter integral. The gradient expansion is the Taylor expansion in  $k^2$

$$I(k^2, m_1, m_2) = I_1(m_1, m_2) + I_2(m_1, m_2)k^2 + \dots$$

with

$$\begin{aligned} I_1(m_1, m_2) &= I(0, m_1, m_2) = \frac{\ln\left(\frac{m_1^2}{m_2^2}\right)}{m_1^2 - m_2^2} = \frac{\ln\left(\frac{m_2^2}{m_1^2}\right)}{m_2^2 - m_1^2}, \\ I_2(m_1, m_2) &= \frac{\partial}{\partial(k^2)} I(k^2, m_1, m_2) \Big|_{k^2=0} \\ &= \frac{1}{(m_2^2 - m_1^2)^3} \left[ 2m_1^2 - 2m_2^2 + (m_1^2 + m_2^2) \ln\left(\frac{m_2^2}{m_1^2}\right) \right], \end{aligned}$$

when  $m_1 \neq m_2$  while  $I_1(m, m) = 1/m^2$  and  $I_2(m, m) = 1/(6m^4)$ . With the gradient expansion we return to coordinate space

$$\begin{aligned} \mathcal{A}_{\text{eff}}^{(2)} &= \frac{1}{4\pi} \int d^2 x \left\{ \left[ \mu^2(\mu+1)^2 I_1(2, 2) + 36 I_1(\mu, \mu) \right] \eta_1^2 \right. \\ &\quad + 2\mu^2(\mu+1)^2 I_1(2, \mu) \eta_2^2 \\ &\quad + \left[ \mu^2(\mu+1)^2 I_2(2, 2) + 36 I_2(\mu, \mu) \right] \partial_\mu \eta_1 \partial^\mu \eta_1 \\ &\quad \left. + 2\mu^2(\mu+1)^2 I_2(2, \mu) \partial_\mu \eta_2 \partial^\mu \eta_2 \right\} + \dots \end{aligned} \tag{A.8}$$

In the on-shell renormalization the quadratic terms in  $\mathcal{A}_{\text{eff}}^{(2)}$  are canceled by those in  $\mathcal{L}_{\text{ct}}$ :

$$\begin{aligned} d_1 &= \frac{1}{4} \left[ \mu^2(\mu+1)^2 I_1(2, 2) + 36 I_1(\mu, \mu) \right] \\ d_2 &= 2\mu^2(\mu+1)^2 I_1(2, \mu) \\ d_3 &= -\mu^2(\mu+1)^2 I_2(2, 2) + 36 I_2(\mu, \mu) \\ d_4 &= -2\mu^2(\mu+1)^2 I_2(2, \mu). \end{aligned} \tag{A.9}$$

## References

- [1] E.R.C. Abraham, P.K. Townsend, Nucl. Phys. B 351 (1991) 313.
- [2] M. Cvetič, F. Quevedo, S.J. Rey, Phys. Rev. Lett. 67 (1991) 1836.
- [3] S. Cecotti, C. Vafa, Commun. Math. Phys. 158 (1993) 569.
- [4] D. Bazeia, M.J. dos Santos, R.F. Ribeiro, Phys. Lett. A 208 (1995) 84.
- [5] B. Chibisov, M.A. Shifman, Phys. Rev. D 56 (1997) 7990, Phys. Rev. D 58 (1998) 109901 (Erratum).
- [6] M.A. Shifman, M.B. Voloshin, Phys. Rev. D 57 (1998) 2590.
- [7] D. Bazeia, A.R. Gomes, J. High Energy Phys. 0405 (2004) 012.
- [8] H. Weigel, M. Quandt, N. Graham, Phys. Rev. D 97 (2018) 036017.
- [9] N. Graham, M. Quandt, H. Weigel, Lect. Notes Phys. 777 (2009) 1.
- [10] A. Alonso-Izquierdo, J. Mateos Guilarte, Ann. Phys. 327 (2012) 2251.
- [11] A. Alonso-Izquierdo, W. Garcia Fuertes, M.A. Gonzalez Leon, J. Mateos Guilarte, Nucl. Phys. B 681 (2004) 163.
- [12] A. Alonso-Izquierdo, J.M. Guilarte, J. High Energy Phys. 1401 (2014) 125.
- [13] E. Elizalde, Lect. Notes Phys. Monogr. 35 (1995) 1; K. Kirsten, AIP Conf. Proc. 484 (1999) 106; D.V. Vassilevich, Phys. Rep. 388 (2003) 279.
- [14] R.F. Dashen, B. Hasslacher, A. Neveu, Phys. Rev. D 10 (1974) 4114.
- [15] R. Rajaraman, Solitons and Instantons, North-Holland, 1988.
- [16] N. Graham, R.L. Jaffe, V. Khemani, M. Quandt, M. Scandurra, H. Weigel, Nucl. Phys. B 645 (2002) 49.
- [17] H. Weigel, Phys. Lett. B 766 (2017) 65.
- [18] A. Alonso-Izquierdo, J. Mateos Guilarte, Nucl. Phys. B 852 (2011) 696.
- [19] M.A. Lohe, Phys. Rev. D 20 (1979) 3120; M.A. Lohe, D.M. O'Brien, Phys. Rev. D 23 (1981) 1771.
- [20] N. Graham, R.L. Jaffe, M. Quandt, H. Weigel, Phys. Rev. Lett. 87 (2001) 131601.
- [21] E. Farhi, N. Graham, R.L. Jaffe, H. Weigel, Nucl. Phys. B 585 (2000) 443.